Journal of Computer-Aided Molecular Design, 9 (1995) 226–236
ESCOM

J-CAMD 290

Simulation analysis of formycin 5'-monophosphate analog substrates in the ricin A-chain active site

Mark A. Olson*, John P. Scovill and Dallas C. Hack

Department of Cell Biology and Biochemistry, U.S. Army Medical Research Institute of Infectious Diseases, Frederick, MD 21702-5011, U.S.A.

Received 28 March 1994
Accepted 29 November 1994

Keywords: Ricin; *N*-glycosidase; Enzyme–ligand complex; Molecular dynamics; Structural interactions; Binding free energies

Summary

Ricin is an RNA *N*-glycosidase that hydrolyzes a single adenine base from a conserved loop of 28S ribosomal RNA, thus inactivating protein synthesis. Molecular-dynamics simulation methods are used to analyze the structural interactions and thermodynamics that govern the binding of formycin 5'-monophosphate (FMP) and several of its analogs to the active site of ricin A-chain. Simulations are carried out initiated from the X-ray crystal structure of the ricin–FMP complex with the ligand modeled as a dianion, monoanion and zwitterion. Relative changes in binding free energies are estimated for FMP analogs constructed from amino substitutions at the 2- and 2'-positions, and from hydroxyl substitution at the 2'-position.

Introduction

The plant toxin ricin is among the most cytotoxic substances known [1,2]. Isolated from the seeds of the castor bean plant (*Ricinus communis*), the cytotoxicity of ricin was first described over a century ago [3]. Structurally, ricin is a heterodimeric protein of the form A:B. The B-chain (RTB) is a cell-surface, receptor-binding protein of 262 residues that mediates the entry of the 267-residue cytotoxic A-chain (RTA) into the cytoplasm [4]. Once internalized, RTA acts catalytically to inactivate eukaryotic 80S ribosomes by damaging a site on the 60S subunit, thus preventing protein synthesis [5,6]. Depending on the source of ribosomes and assay conditions, RTA displays k_{cat} and K_m values in the ranges of 300–1500 min^{-1} and 0.1–1.3 μM, respectively [7,8]. The A-chain catalytically inactivates 28S ribosomal RNA by cleaving a single specific *N*-glycosidic bond among approximately 7000 nucleoside residues; the site of cleavage is A-4323 in the sequence AGUACGA*GAGAGGAAC [9,10].

Amino acid sequence comparisons show that the A-chain is homologous to a large class of single-chain plant ribosome-inhibiting proteins which function by the same *N*-glycosidase mechanism [11]. Examples include trichosanthin [12], Mirabilis and pokeweed antiviral proteins [13–15], saporin-6 [16] and the protein synthesis inhibitor from barley seeds [17]. In addition, RTA is homologous with bacterial toxins such as the Shiga toxins produced from *Shigella disentaria* [18] and *Escherichia coli* [19].

The X-ray crystal structure of RTA at a refinement of 2.5 Å was recently reported by Robertus and co-workers [20,21], and an active-site cleft has been identified. The molecule folds into three compact domains, each characterized by their structural motifs and interactions. The N-terminal domain (residues 1–117) contains all β-sheets in the structure plus two α-helices. The second domain (residues 118–210) contains five α-helices; the C-terminal domain is primarily random coil, with one helix. The central feature of the RTA molecule is a long α-helix involved in creating or stabilizing the active site, which consists of eight invariant residues and five highly conserved polar residues. There are two cysteine residues with one disulfide bridge linking RTB.

Using the three-dimensional structure of RTA and sequence homologies, a number of site-directed mutants have been constructed aimed at determining the mechanism of action. Of particular importance are the invariant residues Glu^{177} and Arg^{180}. The conversion of Glu^{177} to the

*To whom correspondence should be addressed.

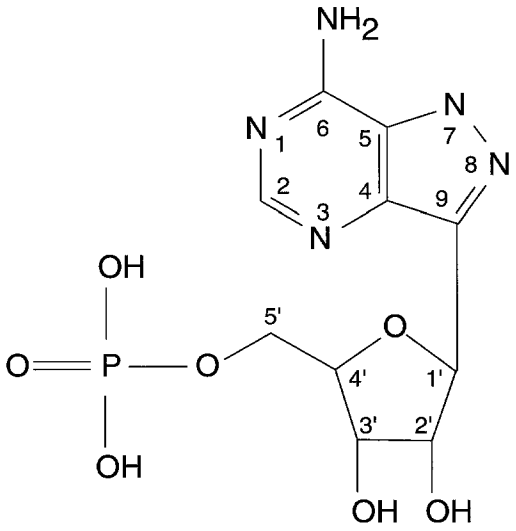

Fig. 1. Chemical structure of formycin 5'-monophosphate.

corresponding amide decreases activity 180-fold [8] and the conversion of Arg^{180} to histidine results in a nearly 1000-fold reduction in activity [22]. Other key RTA mutants include single-site substitutions of phenylalanine for Tyr^{80}, Tyr^{123} and Trp^{211}, resulting in decreased activity by factors of 7 to 15 [8,23], and the conversion of Asn^{209} to serine, decreasing activity threefold [8]. The latter residues are believed to be critical for the cooperative tight binding of the ribosome. From the mutagenic studies, a mechanism of action has been proposed involving the transition-state stabilization of an oxycarbonium ion on the ribose by interaction with Glu^{177} and protonation of adenine by Arg^{180} [8,24].

Recently, the active site of RTA was characterized from the X-ray structure of the binding of formycin 5'-monophosphate (FMP) and adenylyl-3',5'-guanosine (ApG) [24], two nucleotide ligands thought to mimic certain structural interactions of the rRNA substrate. The ligand FMP has been shown by Schramm and co-workers [25, 26] to be a strong competitive inhibitor of the mechanistically related enzyme, AMP nucleosidase, to which it binds 1200- to 2600-fold more tightly (depending on the source of the enzyme) than the normal substrate, AMP. The tight binding of FMP (attributed to a *syn* conformational binding mode [27]) and its structural similarity to AMP suggest that FMP may be a transition-state analog for the *N*-glycosidase reaction. For ricin A-chain, however, it has been shown that FMP is not an inhibitor, nor a strong binding ligand [24]. Moreover, the X-ray crystal structure suggests that FMP does not bind in a transition-state structure. The binding affinity of ApG for RTA appears to be less than that of FMP [24].

The ability of ricin A-chain to recognize and bind both FMP and ApG provides a computational framework for exploring the possible design of a nucleoside with a strong binding affinity and perhaps function as a template for the development of a ricin inhibitor. In this paper, we present a molecular-dynamics (MD) simulation study of the structural interactions and thermodynamics that govern the binding of FMP and several analog derivatives with the RTA active site. Simulations were initiated from the X-ray crystal structure of the RTA–FMP complex and relative free energies of binding were estimated using a thermodynamic integration technique [28], applied to FMP analogs constructed from amino and hydroxyl substitutions at the 2-position of the pyrazolopyrimidine moiety (see Fig. 1), and from amino substitution at the ribose 2'-position. Because of the lack of specific interactions of the FMP phosphate group with protein atoms observed in the X-ray structure, combined with the ambiguity in treating the ionization state of FMP within the RTA active site, several different simulation models of the enzyme–ligand complex were considered, corresponding to full and partial ionization of the phosphate group, as well as a zwitterion in which N-3 of the formycin ring was protonated, as suggested by the known X-ray crystal structure of unbound FMP [27]. Structural binding interactions for each of the simulation models together with the crystal structure were characterized at the level of electrostatic and van der Waals interactions for key individual residues in the RTA active site.

Computational methods

To estimate the relative binding affinity of formycin monophosphate and its analogs (denoted as FMP') with the active site of RTA, we employ the following thermodynamic cycle:

$$\begin{array}{ccc} \text{RTA} + \text{FMP} & \xrightarrow{\Delta A_{inhib}} & \text{RTA:FMP} \\ \Delta A_{solv} \downarrow & & \downarrow \Delta A_{bind} \\ \text{RTA} + \text{FMP}' & \xrightarrow[\Delta A'_{inhib}]{} & \text{RTA:FMP}' \end{array}$$

where ΔA_{inhib} and $\Delta A'_{inhib}$ are the Helmholtz free energies of binding for substrates FMP and FMP', respectively; ΔA_{solv} represents the solvation free-energy difference between FMP and FMP', and ΔA_{bind} represents the binding free-energy difference between FMP and FMP' in the RTA active site. The desired relative free-energy change is given by $\Delta(\Delta A) = \Delta A'_{inhib} - \Delta A_{inhib} = \Delta A_{bind} - \Delta A_{solv}$. The computational method employed in calculating ΔA_{bind} and ΔA_{solv} is based on statistical mechanical perturbation theory [29], implemented via a finite-difference thermodynamic integration algorithm [28].

Molecular-dynamics simulations were performed for a series of small discrete transformations of FMP into the 2- and 2'-amino and 2-hydroxyl analogs, using the pro-

gram DISCOVER [30]. Calculations included both forward and backward perturbations with parameterization of the Hamiltonian carried out at the level of the force-field parameters. The force fields were modeled using the Consistent Valence Force Field (CVFF) [31], which consists of a sum of bond length, bond angle, improper torsion, dihedral angle, electrostatic and van der Waals terms. Partial atomic charges used in the ligand simulation models were derived to yield ionic charges corresponding to a dianion, monoanion and zwitterion employing the established nucleic acid models in the CVFF calibrated via single-point MNDO [32] calculations. The zwitterionic form is based on the X-ray crystal structure of FMP [25], where the phosphate group was shown to carry a negative charge and the base a positive charge at N-3. The choice of ionization state for RTA amino acid residues aspartate, glutamate, lysine, arginine and histidine corresponds to the pH range between 4 and 5.

The RTA–ligand complex was simulated by constructing an active-site region composed of part of the protein and ligand inside a 12-Å spherical boundary, centered on the initial position of N-3 of FMP as derived from the crystal structure of the RTA–FMP complex (shown in Fig. 2). Amino acid residues lying in the outer shell were rigidly restrained at their initial positions. The active-site region was immersed in an 8-Å layer of water obtained from a reference set previously equilibrated via MD calculations. Any water molecule closer than 1.5 Å to any protein or ligand atom in any one Cartesian direction was deleted. Boundary conditions for the solvent water in the binding complex were modeled using a deformable layer. Water was represented using a flexible SPC potential [33]. Simulations of the enzyme–ligand active-site region consisted of FMP or analog plus 53 RTA residues (1020 protein atoms), sodium counterions depending on the ionic charge of the ligand, and 538 water molecules. Sodium counterions were placed adjacent to the charged phosphate centers to neutralize the anionic systems. For the unbound ligand systems, simulations were carried out by placing the solute from the X-ray crystal structure in a cubic box of length 27 Å, containing 632 water molecules plus counterions. Periodic boundary conditions were utilized in the latter set of calculations to reduce edge effects.

The free-energy simulation protocol for all systems consisted of simulations at 10 values of the advancement coordinate λ connecting the initial (crystal structure) state to the mutated state. The λ_1 simulations were initiated with 400 cycles of minimization using a steepest descent algorithm plus 1000 cycles of minimization via a conjugate gradient algorithm, followed by 10 ps of equilibration. The initial atomic velocities were assigned from a Gaussian distribution corresponding to a temperature of 300 K. Simulations for λ_2, λ_3, ..., λ_9 were carried out following a 5-ps equilibration, starting from the final step of the previous simulation. The λ_{10} simulations were initiated with a 10-ps equilibration. Nonbonded interactions were smoothed to zero beyond 9.0 Å and a constant dielectric ($\varepsilon = 1$) was used. All hydrogens were treated explicitly, employing a 1.0-fs timestep for integrating the equations of motion. The ensemble averages were determined from simulations of 10 ps with coordinates, velocities and energies saved every 50 timesteps (0.05 ps) for further analysis.

To conduct a structural analysis, the average structures for the end-point states (corresponding to $\lambda = 0$ and $\lambda = 1$) were calculated employing a minimization protocol described above, followed by a 30-ps equilibration phase and a 100-ps production calculation. Potential energies arising from the structural interactions between the enzyme and the ligand were calculated employing the CVFF empirical energy function. All simulations were carried out on a CRAY Y-MP located at the National Cancer Institute, Frederick Cancer Research and Development Center.

Results and Discussion

In this section, we present the results and analysis of the structural interactions and thermodynamics underlying the binding of FMP and three of its analogs with the active site of RTA, as calculated from the various simulations described above.

Molecular dynamics of the RTA–FMP complex

We begin with a comparison between the X-ray crystal structure and the average MD simulation structure of the dianion model system for the binding complex RTA–FMP. Table 1 summarizes the averaged intramolecular and nonbonded interaction energies computed over 100 ps for the simulation model and the corresponding values for the X-ray structure. The nonbonded electrostatic interactions are an energy contribution that shows significant deviation between RTA and FMP. Superposition of the X-ray structure and the simulation structure (shown in Fig. 3) illustrates key structural similarities, as well as noticeable differences. In accord with the crystal structure, the simulation shows the formycin ring to be conformationally stacked between the rings of Tyr^{80} and Tyr^{123}. Both residues have strong packing interactions with the ligand; calculated van der Waals structural interaction energies for the simulation structure are –5.7 and –2.7 kcal/mol for Tyr^{80} and Tyr^{123}, respectively, and for the X-ray structure, these values are –4.4 and –2.4 kcal/mol, respectively. In both structures, the hydroxyl group of Tyr^{80} further contributes to the binding of the formycin ring by making several distant (3.0 to 4.8 Å) electrostatic interactions with N-6 and N-7, along with the ribose O-4'. The difference in nonbonded structural interaction energies calculated from the two structures for residues 80 and 123 is 2.4 kcal/mol, favoring the simulation structure.

Both in the crystal structure and in the average simulation structure, FMP strongly interacts with polar groups of the active-site cavity. Most important are several backbone carbonyls that point toward the center of positive charge density of the formycin ring and form hydrogen bonds to its protons. The crystal structure and the simulation structure both show N-6 donating a hydrogen bond to the carbonyls of Val^{81} and Gly^{121}, and a hydrogen bond between N-7 and the carbonyl of Gly^{121}. In addition, both structures show N-1 accepting a hydrogen bond from the backbone amide group of Val^{81}. The sum of the electrostatic and van der Waals interaction energies for Val^{81} and Gly^{121} is −3.4 kcal/mol in the crystal structure and −3.7 kcal/mol in the simulation structure.

The average simulation structure for the dianion model is in further agreement with the crystal structure, showing FMP interacting with charged residues of the active site, principally Glu^{177}, Arg^{180} and Glu^{208}. Residues 177 and 180 are located near the C-terminus of an α-helix, which contains a distinct bend allowing the side chains of both residues to reach the molecular surface of the active-site cavity. In the simulation structure, the two residues form an ion-pair interaction similar to the interactions observed in the unbound enzyme crystal structure [20] and the full MD simulation structure (M.A. Olson, unpublished data). The guanidinium group of Arg^{180} donates a strong hydrogen bond to N-3 of the formycin ring. Aggregate electrostatic interactions between Arg^{180} and the ligand are −6.4 kcal/mol in the crystal structure and −39.0 kcal/mol in the simulation structure. The calculated difference can be attributed to greater interactions with the charged phosphate group in the simulation model (see discussion below). In the simulation structure, the carboxylate of Glu^{177} and the backbone carbonyl of Glu^{208} make strong electrostatic interactions with the ribose O-2' and O-3', respectively, resulting in a combined −16.1 kcal/mol electrostatic interaction. Molecular-dynamics simulations of point mutations Arg^{180} to histidine and Glu^{177} to glutamine indicate significant destabilizing free-energy interactions, decreasing the relative binding affinity of FMP (M.A. Olson, unpublished data). In the X-ray structure, the ribose O-2' appears to interact weakly (−1.2 kcal/mol) with both Glu^{177} and Glu^{208}.

Both the simulation structure and the crystal structure show contributions to the binding of the ligand by the side chain of Ile^{172} and amide groups of Asn^{122}, Trp^{211} and Gly^{212}. Ile^{172} packs against the formycin ring and makes favorable van der Waals interactions of −1.9 kcal/mol in the crystal structure and −1.6 kcal/mol in the simulation structure. The amide backbones of residues 122, 211 and 212 exert their effect on the binding of FMP primarily through long-range electrostatic interactions with N-7 (residue 122) and both the ribose O-3' and phosphate group (residues 211 and 212). The combined effect of these backbone electrostatic interactions is −9.4 kcal/mol in the X-ray structure and −19.3 kcal/mol in the average simulation structure. Finally, Trp^{211} has been shown to undergo a large increase in fluorescence upon adenine binding to the RTA active site [34]. The simulation structure shows weak van der Waals interactions between the tryptophan ring and C-5' of FMP. Both the crystal structure and the simulation structure of the enzyme–ligand complex, as well as the unbound enzyme structure [20], show Trp^{211} near a (t,−) rotameric state, leading to negligible conformational change of residue 211 due to FMP binding.

Structural differences between the X-ray crystal structure and the average simulation structure for the dianion model system are derived primarily from electrostatic interactions between the phosphate group and protein atoms. In the X-ray structure, the phosphate group pro-

TABLE 1
COMPARISON OF INTRAMOLECULAR AND INTERACTION ENERGIES OF THE FMP SUBSTRATE FOR THE X-RAY STRUCTURE AND SIMULATION MODELS[a]

Energy (kcal/mol)	Dianion		Monoanion		Zwitterion	
	X-ray	Simulation	X-ray	Simulation	X-ray	Simulation
Intramolecular						
angle	49.9	51.4 (0.5)	50.7	52.9 (2.9)	55.8	56.9 (0.1)
dihedral	5.7	15.5 (3.5)	6.8	15.7 (1.9)	7.5	17.1 (1.9)
bond	38.4	23.3 (5.7)	33.2	23.4 (2.9)	30.7	22.6 (0.3)
X-term	−3.2	−2.5 (0.2)	−3.4	−2.1 (1.2)	−3.2	−1.0 (0.7)
electrostatic	−3.3	15.0 (2.0)	−73.6	−72.7 (1.7)	−44.3	−104.2 (1.4)
van der Waals	48.2	38.3 (2.7)	48.7	37.7 (3.1)	48.2	31.0 (4.8)
total	135.8	140.8 (6.2)	62.2	54.9 (11.9)	94.7	22.5 (9.2)
Interaction						
electrostatic	−67.8	−152.8 (1.8)	−41.7	−116.6 (8.5)	−36.6	−218.3 (7.4)
van der Waals	−15.3	−20.2 (1.9)	−15.3	−19.0 (0.2)	−15.3	−13.4 (0.4)
total	−83.1	−173.0 (0.1)	−57.0	−135.7 (8.7)	−51.9	−231.7 (7.0)

[a] Values for the X-ray structure were calculated using partial atomic charges of the corresponding simulation model. Simulation values listed were averaged over 100 ps; the values in parentheses indicate the pertinent standard deviation.

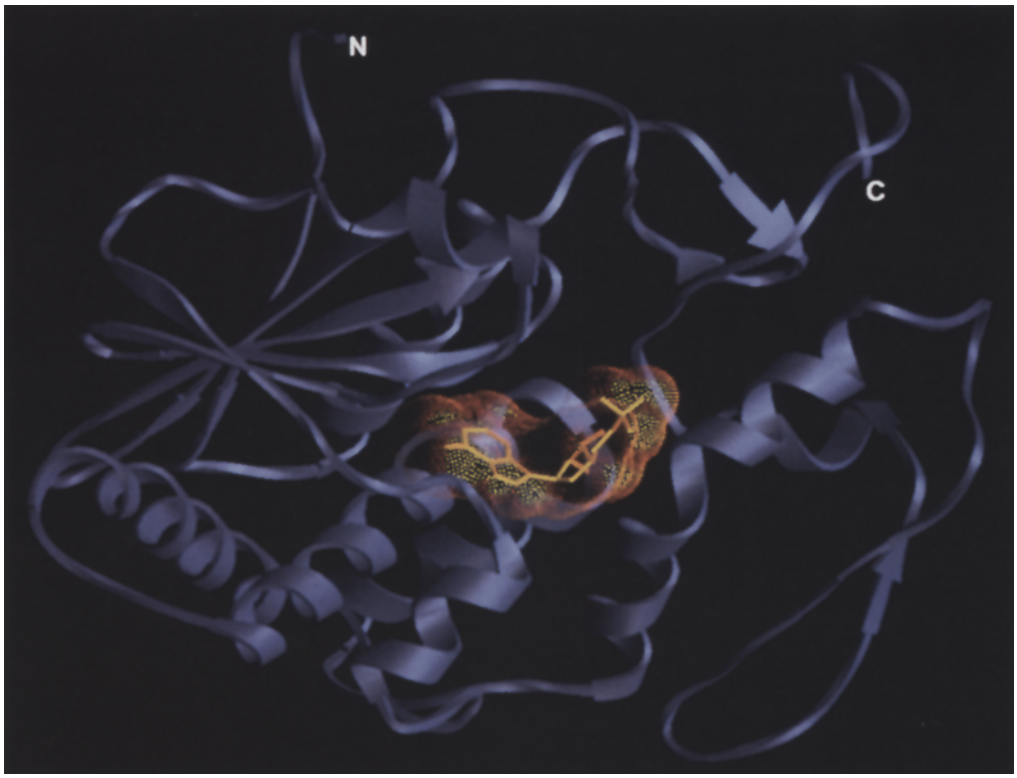

Fig. 2. Ribbon representation of the binding complex of ricin A-chain (violet) with formycin 5'-monophosphate (gold).

jects out of the binding pocket into the solvent and makes a long-range (4.7 Å) electrostatic interaction with the positively charged guanidinium group of Arg^{258}. The average simulation structure shows the phosphate group at a lower position as a result of optimizing ion-pair interactions with Arg^{258} and long-range interactions with Arg^{180}. The electrostatic interactions between FMP and Arg^{258} corresponding to the crystal structure and the simulation structure are –40.3 and –70.6 kcal/mol, respectively.

The average simulation structure shows the phosphate group strongly interacting with eight water molecules, three of which form bridges with side chains of Tyr^{80}, Gly^{212} and Arg^{258}. Because of strong electrostatic interactions of the phosphate group with protein atoms, as described above, the simulation structure suggests a less restrictive solvent-accessible surface area for the sugar than observed in the crystal structure, showing two possible hydrogen bonds with water molecules, one bridging Gly^{212} and the phosphate group. The simulation also clearly shows the desolvation of several key active-site residues upon binding of FMP. A comparison of the RTA–FMP simulation structure with the average MD simulation structure of the free enzyme (M.A. Olson, unpublished data) shows the loss of approximately five water molecules bound to residues Glu^{177}, Arg^{180} and Glu^{208}. These waters are thought to be critical nucleophiles in the development of a transition-state-like binding complex of the ribosomal RNA [20,21].

Figure 4 shows structures of FMP in the RTA active site during the 100-ps MD simulation. The phosphate backbone and the formycin ring showed noticeable thermal fluctuations during the simulation, while the sugar remained relatively rigid along the ribose O-4' backbone and somewhat flexible in the hydroxyl groups. Table 2 lists a comparison of the torsion angles describing the conformation of FMP obtained from the X-ray structure and the average simulation structure. The calculated backbone torsion angles β and γ show deviations from the crystal structure of about 103° and 23°, respectively which, as discussed above, can be attributed to the significant interactions between protein atoms and the phosphate group of the simulation model. The simulation structure shows exocyclic and endocyclic torsions corresponding to a 2'-*endo* pucker, in contrast to the 3'-*endo* configuration observed in the crystal structure, although the uncertainty in the crystallographic density makes accurate determinations very difficult. Calculated endocyclic torsions appear to be driven by interactions of the ribose ring with Glu^{177} and Glu^{208}. In the crystal structure, the formycin ring exhibits a high *syn* configuration with a torsion χ of about 128°, whereas the simulation model shows χ having a value near 80° ± 10°.

Given the MD simulation results of the dianion model system, in particular the interactions of the phosphate group, coupled with the uncertainty in modeling the protonation state of the formycin ring in the active site of

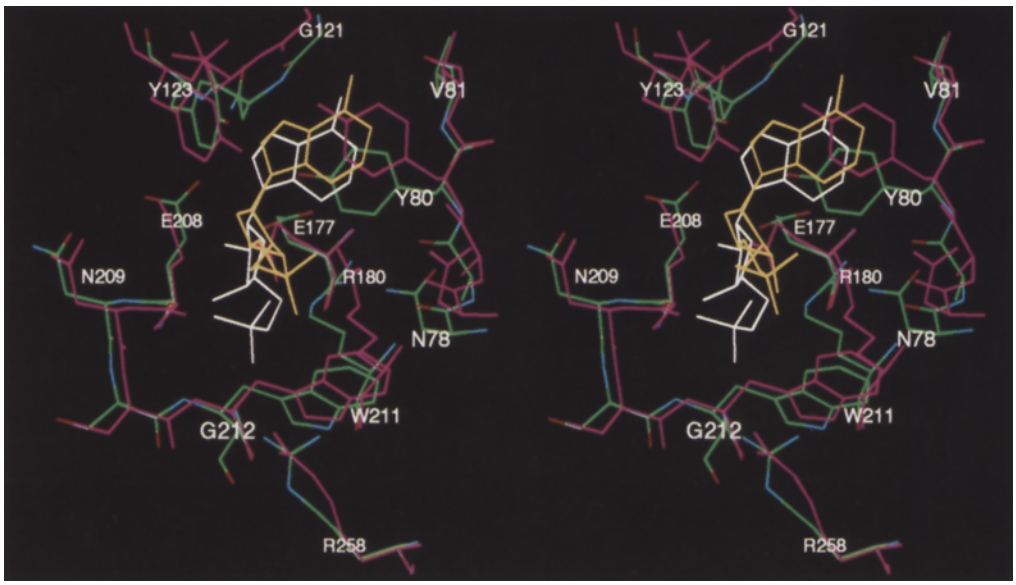

Fig. 3. Stereoview showing a superposition of the average dianion model simulation structure and the X-ray crystal structure for the binding RTA–FMP complex. Color coding: simulation FMP, white; X-ray FMP, yellow; simulation RTA carbon, green; nitrogen, blue; oxygen, red; X-ray RTA, magenta.

RTA, sets of simulations were carried out for monoanionic and zwitterionic ligand structures. From Table 1, it can be seen that the electrostatic interaction energy computed for the monoanion model shows a significant deviation from the crystal structure, as was found with the dianion simulation model. A superposition of the X-ray crystal structure and the average simulation structure is shown in Fig. 5. The simulation structure is found to be similar to the dianion model, showing a binding mode of FMP involving Tyr^{80} and Tyr^{123} through strong van der Waals interactions of –4.6 and –2.8 kcal/mol, respectively. The backbone carbonyls of Val^{81} and Gly^{121}, along with the amide group of Val^{81}, form combined electrostatic interactions with FMP of –1.7 kcal/mol. The most noticeable difference, as expected, is in the interactions of the phosphate group with surrounding protein atoms. Interaction of FMP with the guanidinium group of Arg^{258} is reduced on average by 25 kcal/mol compared to the dianion model. Accompanying this reduction is a favorable increase in long-range electrostatic interactions between the phosphate group and Arg^{213}, made possible in part by a reduction in the number of water molecules (from eight to four) solvating the phosphate moiety. Residues 177 and 208 appear to form strong hydrogen bonds with the hydroxyl groups of the sugar; the combined electrostatic interaction roughly amounts to –14.9 kcal/mol, in agreement with the dianion model. For Arg^{180}, there appears to be a reduction in the magnitude of the electrostatic inter-

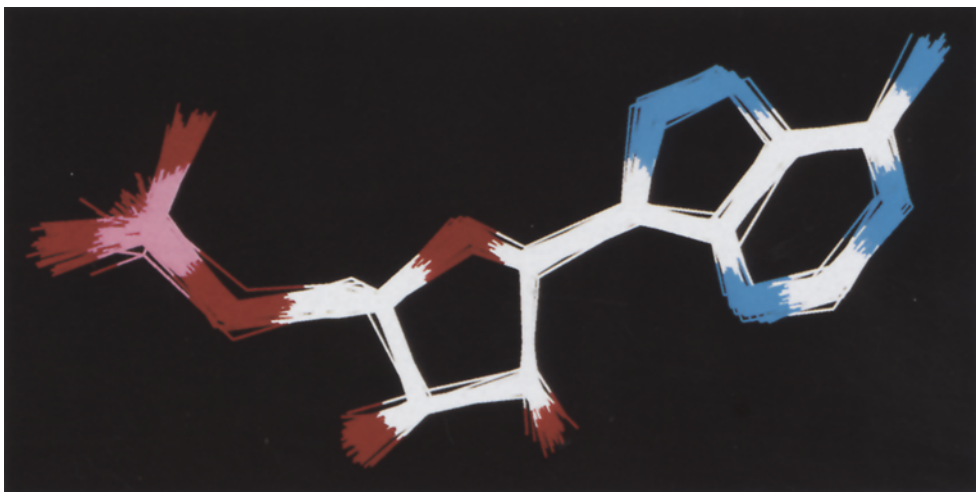

Fig. 4. Molecular structures of the dianion formycin 5'-phosphate observed in the ricin A-chain active site, immersed in solvent water during 100 ps of molecular dynamics. The 50 superimposed structures were observed at 2.0 ps intervals. Color coding of atoms: carbon, white; nitrogen, blue; oxygen, red; phosphate, magenta.

actions with the ribose and phosphate groups, showing a potential energy of −46.0 kcal/mol.

From Table 2, the calculated backbone torsion angles β and γ for the monoanion model appear to deviate from the crystal structure by about 23° and 16°, respectively. The calculated exocyclic torsion angle δ is near the value calculated in the dianion model. The endocyclic torsions show somewhat better agreement with the crystal structure values than the dianion model results and the formycin ring appears to be in a high *syn* configuration with a torsion χ of about 130° ± 19°.

Simulation results for the zwitterion model show significant deviation from the X-ray crystal structure in the interactions and conformations of FMP and several active-site residues (Table 1 and Fig. 5). Protonation of N-3 produces an approximate 3-Å shift and 40° rotation of the formycin ring from the average simulation monoanionic structure. The van der Waals structural interaction energy contributions for residues 80 and 123 are calculated to be about −1.8 and −1.5 kcal/mol, respectively. These values are substantially reduced compared to the crystal structure and the anion model simulations. Likewise, total nonbonded interactions between N-6 and the backbone carbonyl of Val^{81} are reduced significantly. The average simulation structure of the zwitterion model shows Gly^{121} making a hydrogen bond with N-6, rather than N-7 as in the anion model results, and several strong long-range electrostatic interactions between the formycin ring and Asp^{75}, Asp^{96} and Asp^{100}. Interactions with these latter residues, made possible by the rotational shift in the formycin ring, contribute roughly −45 kcal/mol to the total electrostatic interactions and reflect a different binding mode of the formycin ring with the ricin active site. Several hydrogen bonds are present between the carboxylate of Glu^{177} and protons at N-3 and O-2'. The calculated electrostatic interaction energy for residue 177 is considerably larger than in the crystal structure and in simulation structures for the anion models, and is accompanied by a significant change in the conformation of the residue. The simulation structure also shows two strong hydrogen bonds between Arg^{180} and N-3, plus a hydrogen bond between the backbone carbonyl of Glu^{208} and the proton at O-3'. Strong electrostatic interactions are present between the phosphate group and Arg^{213} and Arg^{258}, as found in the monoanion simulation model results.

From Table 2, it can be seen that the calculated angles β and γ for the zwitterion simulation model show deviations from the crystal structure of roughly 51° and 7°, respectively. The calculated backbone angle δ is 152°, showing a substantial disagreement with the observed crystal structure. Further significant deviations are observed for the ribose endocyclic torsions, while the formycin ring shows a *syn* configuration with a torsion χ of about 141°, which is in approximate agreement with the crystal structure.

A comparison of the three average simulation structures shows that the magnitude of ligand binding interactions with the enzyme increases as zwitterionic > dianionic > monoanionic. As discussed above, all three models predict significantly greater interaction energies than the crystal structure. Furthermore, each of the models predicts an average ligand conformation that differs from the other models and from the crystal structure, both qualitatively and quantitatively. A root-mean-square (rms) superposition of the computed dianionic and monoanionic enzyme–ligand structures indicates a deviation of 0.43 Å, and a fit of the anionic ligand structures with the crystal structure yields an average rms deviation of 0.66 Å. Superpositions of the zwitterionic structure with the monoanionic and crystal structures result in rms deviations of 0.58 and 0.86 Å, respectively. From an examination of the ligand position in the enzyme-binding pocket and the type of structural interactions, the dianion and monoanion simulation models appear to be superior to the zwitterion model in reproducing the enzyme–ligand complex. The zwitterion model, based on the phosphate group carrying a negative charge and the protonation of N-3 of the formycin ring, predicts a ligand structure and binding mode that are inconsistent with the observed RTA–FMP crystal structure.

TABLE 2
COMPARISON OF X-RAY AND COMPUTED TORSION ANGLES FOR FMP IN THE RTA ACTIVE SITE

Torsion angle[a]	X-ray	Dianionic	Monoanionic	Zwitterionic
α	166.2	−153.4 (17.4)[b]	123.7 (14.2)	155.7 (31.3)
β	−173.9	82.8 (7.7)	163.2 (9.6)	135.2 (10.6)
γ	−70.1	−92.9 (6.1)	−86.4 (5.9)	−77.2 (7.5)
δ	75.2	110.9 (6.8)	110.7 (7.8)	151.8 (6.5)
θ_0	44.1	−17.5 (5.2)	6.0 (4.6)	−20.2 (7.0)
θ_1	−40.4	−6.7 (6.0)	−11.0 (5.1)	31.0 (5.6)
θ_2	21.5	30.4 (6.3)	12.2 (8.6)	−31.1 (5.7)
θ_3	6.5	−42.2 (5.8)	−8.5 (10.1)	18.0 (7.2)
θ_4	−31.2	35.6 (5.0)	1.2 (7.9)	2.5 (7.8)
χ	128.1	79.6 (9.5)	130.1 (18.8)	140.7 (9.9)

[a] Listed torsion angles are according to IUPAC nomenclature for backbone torsion angles, ribose endocyclic torsions and the glycosidic torsion.
[b] Values in parentheses indicate the pertinent standard deviation.

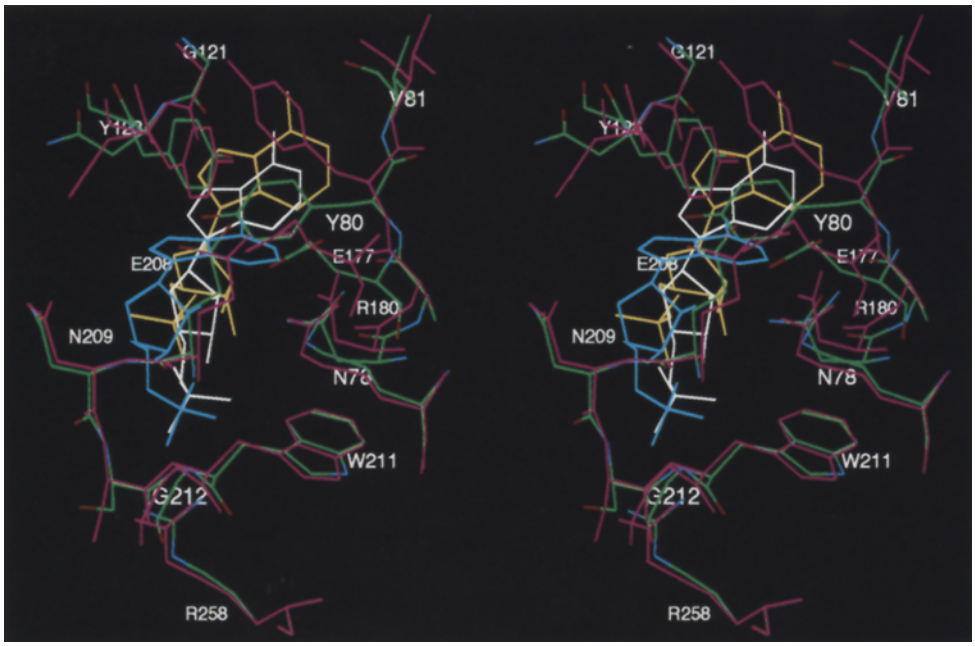

Fig. 5. Stereoview showing a superposition of the average monoanion and zwitterion model simulation structures and the X-ray crystal structure for the binding RTA–FMP complex. Color coding: monoanion simulation FMP, white; zwitterion simulation FMP, cyan; X-ray FMP, yellow; monoanion simulation RTA carbon, green; nitrogen, blue; oxygen, red; zwitterion simulation RTA, magenta.

Finally, it should be noted that the deviations between the X-ray structure and the average simulation structure calculated for a given model possibly arise from a number of sources, e.g. (i) errors in the calculations due to the inherent approximations of the force fields; (ii) errors in the refinement of the crystal structure carried out at 2.8 Å resolution; or (iii) real differences in the binding thermodynamics found in the crystal and in aqueous solution. This latter source of structural differences may be amplified by the observation that FMP exhibits a weak binding affinity, with only 50% occupancy in the ricin crystals [24], and thus may lead to artifactual binding modes from crystallization and/or multiple possible binding modes. This is relevant in particular to the binding

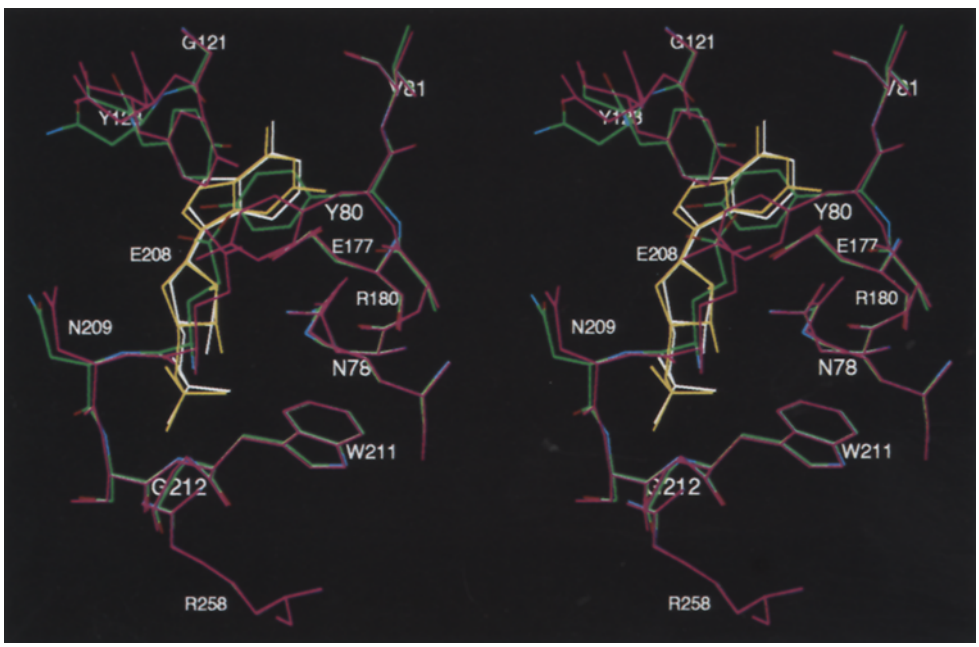

Fig. 6. Stereoview showing a superposition of the average monoanion 2-hydroxyl formycin 5'-phosphate bound in the RTA active site and the monoanion model simulation structure for FMP. Color coding: 2-hydroxyl FMP, yellow; monoanion FMP, white; analog FMP simulation RTA, magenta; monoanion simulation RTA carbon, green; nitrogen, blue; oxygen, red.

TABLE 3
BINDING, SOLVATION AND NET FREE ENERGIES (kcal/mol) FOR FMP ANALOG RTA SUBSTRATES

Transformation	Ionization state	ΔA_{bind}			ΔA_{solv}			$\Delta(\Delta A)$
		Forward	Reverse	Average	Forward	Reverse	Average	
FMP → 2-amino FMP	Dianionic	−15.0	−14.1	−14.5 (0.8)[a]	−21.4	−21.0	−21.2 (0.6)	6.7 (1.4)
FMP → 2-amino FMP	Monoanionic	−25.7	−25.1	−25.4 (0.8)	−32.1	−31.3	−31.7 (0.7)	6.3 (1.5)
FMP → 2-hydroxyl FMP	Dianionic	−9.1	−8.9	−9.0 (0.6)	−11.6	−11.0	−11.3 (0.7)	2.3 (1.3)
FMP → 2-hydroxyl FMP	Monoanionic	−21.2	−20.8	−21.0 (0.7)	−19.4	−19.0	−19.2 (0.7)	−1.8 (1.4)
FMP → 2'-amino FMP	Dianionic	17.5	18.1	17.8 (0.5)	6.7	7.1	6.9 (0.4)	10.9 (0.9)
FMP → 2'-amino FMP	Monoanionic	20.3	20.9	20.6 (0.5)	14.8	15.2	15.0 (0.5)	5.6 (1.0)

[a] Values in parentheses indicate the pertinent standard deviation.

mode of the phosphate group. In comparison, the recent crystal structure of FMP bound to the structurally homologous pokeweed antiviral protein [15] exhibits a 100% occupancy with a similar overall binding mode, except for the phosphate group, which forms a strong ion-pair interaction with Arg^{122} (homologous with RTA Asn^{122}). As described above, the simulation models for the anionic structures predicted similar ion-pair interactions with the nearest equivalent charged residue, Arg^{258}, although less conformationally favorable.

In addition to the inherent approximations of the simulation models, there are other aspects of the calculations that could introduce errors, viz., the truncation of long-range forces, the sphere radius of the active-site region and the computational sampling of conformational space. Requisite testing of these approximations has centered on additional MD simulations of the dianion model system carried out for 300 ps, employing a nonbonded cutoff distance of 11 Å combined with ab initio determined ligand atomic charges, plus an increase in the number of unrestrained RTA residues (M.A. Olson, unpublished data). Simulation results for this model yielded a similar structural displacement of the phosphate group in FMP, as described above. Further examination of the truncation of long-range forces was carried out employing steepest descent minimization of the crystal structure using a 25-Å cutoff, with the results showing a rotational shift in the position of the phosphate group due to an increase in electrostatic interactions with RTA residues. For systems dominated by electrostatic interactions, as in the RTA–FMP complex (see Table 1), implementation of a recently developed extended electrostatic method [35, 36], constructed to approximate the no-cutoff force using a cutoff distance of ~12 Å, into MD simulations may produce a structure with fewer deviations from the X-ray crystal structure. What is important here is that the simulations presented for the anion model systems using a simulation protocol with manageable computational requirements appear to be sufficiently accurate in computing an average structure for the bound ligand which demonstrates an *overall* binding mode similar to the one observed by Monizingo and Robertus [24]. It is important to note, nevertheless, that structure is generally much easier to reproduce than energy and reproducing the RTA–FMP complex is thus a less stringent test of the quality of the parameters employed in the simulations.

Given the above caveats, several structural motifs constructed from the original FMP structure were investigated for the anion models, which by visual inspection of the 3D enzyme–ligand complex may increase the binding affinity for the active site and perhaps yield insight into the development of a transition-state inhibitor for the ricin.

Free-energy simulations

Numerical values obtained from the free-energy simulations of the model systems initiated from the X-ray crystal structure at 300 K are summarized in Table 3. The systematic errors of the simulations were estimated from analyzing the hysteresis derived via forward and backward perturbations. Statistical errors are likely to be much smaller and are on the order of a few tenths of a kilocalorie per mole.

For the 2-amino formycin 5'-phosphate analog transformation, the free energies calculated for the enzyme-bound ligand (ΔA_{bind}) predict the analog to interact more favorably with the enzyme in both the dianion and monoanion simulation models. However, the *relative* binding free energies ($\Delta\Delta A$) predict the 2-amino analog to bind less strongly to RTA than does FMP itself. Selectivity reflects solvation effects, as it is less difficult to desolvate FMP than its 2-amino derivative. The lack of significant sensitivity in the relative free-energy change to the ionization state of the phosphate group suggests a dominate van der Waals component contribution to $\Delta\Delta A$.

In the free-energy simulations for the 2-hydroxyl formycin 5'-phosphate analog, the monoanion model shows a greater relative binding affinity ($\Delta\Delta A = -1.8$ kcal/mol) for the active site of RTA than does the original FMP substrate. Analysis of the average end-point structure (Fig. 6) reveals several changes in the structural interactions between the ligand and residues Tyr^{80}, Glu^{177} and Arg^{180}. Most important, the carboxylate of residue 177 interacts favorably with the hydroxyl group (the net inter-

action energy is about −6.0 kcal/mol). The guanidinium group of Arg^{180} and the carbonyl backbone of Tyr^{80} interact with the hydroxyl group through electrostatic and van der Waals interactions for a combined −1.4 kcal/mol. The formycin ring of the hydroxyl analog appears to be in a high *syn* conformation ($\chi = 150°$) and makes several strong interactions found in the FMP simulation structure, most notably interactions with the polar backbones of Val^{81} and Gly^{121} as well as packing interactions with Tyr^{80} and Tyr^{123}. In the simulation structure, H^{ε} of Arg^{180} makes a strong ion-pair interaction with O-3', and the carboxylate of Glu^{177} and the carbonyl backbone of Glu^{208} form strong hydrogen bonds to protons at the ribose O-2' and O-3', respectively. The ribose structure appears to be in a 3'-*endo* configuration. Both Arg^{213} and Arg^{258} form electrostatic interactions with the phosphate group and contribute significantly to the binding of the hydroxyl analog. Finally, decomposition of ΔΔA shows a large electrostatic free-energy interaction component dominating the improved binding of the ligand.

As for the 2'-amino formycin 5'-phosphate analog, neither of the two simulation models predict a relative increase in binding affinity for the enzyme. Both ΔA_{bind} and ΔA_{solv} show a decrease in favorable interactions with the enzyme and solvent, respectively.

Conclusions

The purpose of these investigations was to analyze the structure and energetics underlying the binding of the ricin A-chain ligand formycin 5'-phosphate and to explore several structural motifs based on the 3D structure which would have a greater binding affinity for the active site. The studies undertaken showed the molecular-dynamics simulation results of the enzyme–ligand complex, employing dianion and monoanion ligand models, to be in good accord with the X-ray crystal structure in reproducing an overall binding mode, unlike the zwitterion model. However, for each of the simulation models there are significant differences in the location and binding of the phosphate group. Simulations predict strong interactions with protein atoms and suggest a pronounced decrease in binding if the phosphate group is removed. It should be noted that a recent attempt to bind 2-amino formycin failed, as revealed by a 3-Å difference Fourier (J. Robertus, private communication). This may be due to either the addition of the amino group or phosphate removal. Free-energy simulation studies showed a preference for FMP over 2-amino formycin 5'-phosphate and 2'-amino formycin 5'-phosphate. The FMP analog 2-hydroxyl formycin 5'-phosphate, modeled as a monoanion, potentially has an improved binding affinity. Two major caveats in evaluating the relative changes in binding free energies are the ambiguity in treating the ionization state of FMP within the RTA active-site cavity and the computational sampling of conformational space, limited here to 100 ps. Regarding the issue why FMP is not a strong binding ligand nor an inhibitor, results from each of the simulation models showed FMP binding strictly in a *syn* conformation, while recent results from an NMR solution structure determination of a ricin-active, GAGA-containing oligoribonucleotide loop indicate that the adenine ring is confined to an *anti* conformation [37]. This suggests a difference in binding surfaces of the two structures surrounding the adenine ring complementary to the RTA active site, as a conformational change in the oligoribonucleotide loop to a *syn* conformation would seem to be energetically unfavorable. Further research is needed in evaluating the importance of this conformational difference for recognition and binding of small ligands. Finally, work is currently in progress aimed at the de novo design of ligands for ricin, employing the simulation results presented in this paper and a rule-based search of small molecules and fragments which may fit the nonbonded contact geometry of the active site [38].

Acknowledgements

We thank J.D. Robertus for supplying the X-ray coordinates of the complexed and native structures, and D.C. Feller, D.M. Ferguson, K.A. Mereish, J.D. Robertus and V.L. Schramm for stimulating discussions. We are grateful to the Biomedical Supercomputing Center, National Cancer Institute, for a generous grant of computer time. The work of M.A.O. was supported by U.S. Army Research Office contract DAAL03-89-C-0038 with the University of Minnesota.

References

1 Eiklid, K., Olsnes, S. and Pihl, A., Exp. Cell Res., 126 (1980) 321.
2 Olsnes, S. and Pihl, A., In Cohen, P. and Van Heyningen, S. (Eds.) Molecular Action of Toxins and Viruses, Elsevier, New York, NY, 1982, pp. 52–105.
3 Stilmark, H., Inaugural Lecture, University of Dorpat, Estonia, 1888.
4 Nicolson, G.L., Lacorbiere, M. and Hunter, T.R., Cancer Res., 35 (1975) 144.
5 Sperti, S., Montanaro, L. and Stripe, F., Biochem. J., 136 (1973) 813.
6 Endo, Y. and Tsurugi, K., J. Biol. Chem., 262 (1987) 8128.
7 Olsnes, S., Fernadez-Puentes, C., Carrasco, L. and Vasquez, D., Eur. J. Biochem., 60 (1975) 281.
8 Ready, M.P., Kim, Y. and Robertus, J.D., Proteins, 10 (1991) 270.
9 Endo, Y., Mitsui, K., Motizuki, M. and Tsurugi, K., J. Biol. Chem., 262 (1987) 5908.
10 Glück, A., Endo, Y. and Wool, I.G., J. Mol. Biol., 226 (1992) 411.
11 Endo, Y., Tsurugi, K. and Lambert, J.M., Biochem. Biophys. Res. Commun., 150 (1988) 1032.

12 Collins, E.J., Robertus, J.D., LoPreti, M., Stone, K.L., Williams, K.R., Wu, P., Hwang, K. and Piatak, M., J. Biol. Chem., 265 (1990) 8665.
13 Habuka, N., Murakami, Y., Noma, M., Kudo, T. and Horikoshi, K., J. Biol. Chem., 264 (1989) 6629.
14 Ready, M., Wilson, K., Piatak, M. and Robertus, J.D., J. Biol. Chem., 259 (1984) 15252.
15 Monzingo, A.F., Collins, E.J., Ernst, S.R., Irvin, J.D. and Robertus, J.D., J. Mol. Biol., 233 (1993) 705.
16 Benatti, L., Saccardo, M., Dani, M., Nitti, G., Sassano, M., Lorenzetti, R., Lappi, D. and Soria, M., Eur. J. Biochem., 183 (1989) 465.
17 Asano, K., Svensson, B., Svendsen, I., Poulsen, P. and Roepstorff, P., Carlsberg Res. Commun., 51 (1986) 129.
18 O'Brien, A.D. and Holmes, R.K., Microbiol. Rev., 51 (1987) 206.
19 Calderwood, S.B., Auclair, F., Donohue-Rolfe, A., Keusch, G.T. and Mekalanos, J.J., Proc. Natl. Acad. Sci. USA, 84 (1987) 4364.
20 Katzin, B.J., Collins, E.J. and Robertus, J.D., Proteins, 10 (1991) 251.
21 Rutenber, E., Katzin, B.J., Collins, E.J., Mlsna, D., Ernst, S.E., Ready, M.P. and Robertus, J.D., Proteins, 10 (1991) 240.
22 Frankel, A., Welsh, P., Richardson, J. and Robertus, J.D., Mol. Cell. Biol., 10 (1990) 6257.
23 Bradley, J.L. and McGuire, P.M., Int. J. Pept. Protein Res., 35 (1990) 365.
24 Monzingo, A.F. and Robertus, J.D., J. Mol. Biol., 227 (1992) 1136.
25 DeWolf Jr., W.E., Fullin, F.A. and Schramm, V.L., J. Biol. Chem., 254 (1979) 10868.
26 Leung, H.B. and Schramm, V.L., Biochemistry, 255 (1980) 10867.
27 Giranda, V.L., Berman, H.M. and Schramm, V.L., Biochemistry, 27 (1988) 5813.
28 Beveridge, D.L. and Dicapua, F.M., In Van Gunsteren, W.F. and Weiner, P.K. (Eds.) Computer Simulation of Biomolecular Systems, Vol. 1, ESCOM, Leiden, 1989, pp. 1–26.
29 Zwanzig, R.W., J. Chem. Phys., 22 (1954) 1420.
30 DISCOVER, Version 2.9, Biosym Technologies, Inc., San Diego, CA, 1993.
31 Dauber-Osguthorpe, P., Roberts, V.A., Osguthorpe, D.J., Wolff, J., Genest, M. and Hagler, A.T., Proteins, 4 (1988) 31.
32 Stewart, J.J.P., MOPAC 5.0, QCPE Bull., 9 (1989) 123.
33 Teleman, O., Jönsson, B. and Engström, S., Mol. Phys., 60 (1987) 193.
34 Watanabe, K., Honjo, E., Tsukamoto, T. and Funatsu, G., FEBS Lett., 304 (1992) 249.
35 Stote, R.H., States, D.J. and Karplus, M., J. Chem. Phys., 88 (1991) 2419.
36 Straub, J.E., Lim, C. and Karplus, M., J. Am. Chem. Soc., 116 (1994) 2591.
37 Szewczak, A.A., Moore, P.B., Chan, Y.-L. and Wool, I.G., Proc. Natl. Acad. Sci. USA, 90 (1993) 9581.
38 Böhm, H.-J., J. Comput.-Aided Mol. Design, 6 (1992) 61.